

## Article

# Investigations on Microstructures and Properties of (Fe, Cr, W)<sub>7</sub>C<sub>3</sub> Carbides by First Principles and Experiments

Chao Chen <sup>1</sup>, Junfa Wang <sup>1,\*</sup>, Yiyuan Ge <sup>2</sup> and Lili Ma <sup>2</sup><sup>1</sup> School of Materials Science and Engineering, Jiamusi University, Jiamusi 154007, China<sup>2</sup> School of Mechanical Engineering, Jiamusi University, Jiamusi 154007, China

\* Correspondence: wangjunf2934@sina.com

**Highlights:**

- The structural and elastic properties of (Fe, Cr, W)<sub>7</sub>C<sub>3</sub> were investigated by first principles.
- Tungsten doping can improve the ductility and the indentation modulus of (Fe, Cr)<sub>7</sub>C<sub>3</sub> carbides.
- The elastic anisotropy of M<sub>7</sub>C<sub>3</sub> became weaker after tungsten doping.
- A new carbide (Fe<sub>3.27</sub>Cr<sub>2.99</sub>W<sub>0.74</sub>)C<sub>3</sub> was found to be a combination of mechanical properties.

**Abstract:** Tungsten doping is critical for the wear resistance and application of High-Chromium Cast Iron (HCCI). A series of investigations of (Fe, Cr, W)<sub>7</sub>C<sub>3</sub> carbides were performed by first principles calculations and experimental analysis. The calculated results showed that with the increase in tungsten content in M<sub>7</sub>C<sub>3</sub>, the equilibrium cell volumes and the density gradually increased, and the formation energy of M<sub>7</sub>C<sub>3</sub> carbides gradually decreased. The TEM results showed that the (Fe, Cr, W)<sub>7</sub>C<sub>3</sub> carbides were (Fe<sub>3.27</sub>Cr<sub>2.99</sub>W<sub>0.74</sub>)C<sub>3</sub> with a hexagonal structure after adding 2.13 wt % tungsten into laser cladding coatings of High-Chromium Cast Iron with a composition of Fe-26.8 wt % Cr-3.62 wt % C. These results from calculations and in situ nanoindentation show that tungsten doping could improve the ductility and indentation modulus of (Fe, Cr)<sub>7</sub>C<sub>3</sub> carbides, and the composition of (Fe, Cr, W)<sub>7</sub>C<sub>3</sub> was expected to be a high hardness and softness material. The wear test results showed that the wear resistance of tungsten-bearing HCCI was better than ordinary HCCI.

**Keywords:** (Fe, Cr, W)<sub>7</sub>C<sub>3</sub>; HCCI; first principles calculations; laser cladding coatings; nanoindentation



**Citation:** Chen, C.; Wang, J.; Ge, Y.; Ma, L. Investigations on Microstructures and Properties of (Fe, Cr, W)<sub>7</sub>C<sub>3</sub> Carbides by First Principles and Experiments. *Coatings* **2022**, *12*, 1363. <https://doi.org/10.3390/coatings12091363>

Academic Editor: Aivaras Kareiva

Received: 30 July 2022

Accepted: 16 September 2022

Published: 18 September 2022

**Publisher's Note:** MDPI stays neutral with regard to jurisdictional claims in published maps and institutional affiliations.



**Copyright:** © 2022 by the authors. Licensee MDPI, Basel, Switzerland. This article is an open access article distributed under the terms and conditions of the Creative Commons Attribution (CC BY) license (<https://creativecommons.org/licenses/by/4.0/>).

## 1. Introduction

Hypereutectic High-Chromium Cast Iron (HCCI) is an important wear resistance material, widely used in the mining and crushing field due to its easy production, low cost and excellent wear resistance [1–3]. The microstructure of HCCI primarily contains hard M<sub>7</sub>C<sub>3</sub>-type carbides (with a high hardness of 1300–1800 HV) and martensitic matrix [4]. There are three types of HCCI: hypoeutectic HCCI, eutectic HCCI and hypereutectic HCCI [5]. For hypereutectic HCCI, the M<sub>7</sub>C<sub>3</sub> eutectic carbides solidify firstly, and could improve the hardness and the wear resistance of HCCI. HCCI could be prepared by casting [6], an Electrothermal Exial Plasma Accelerator (EAPA) [7] and so on. Heydari et al. [6] prepared HCCI with 22% Cr, 10%–12% tungsten by casting. The results showed that the coarse chromium carbides are distributed in the matrix when the carbon content was low (2.3 wt %). With the increase in carbon content, the carbides will become finer. Efremenko et al. [7] studied the effect of layered morphology and heat treatment on the microstructure and hardness after the pulsed plasma deposition of Fe-C-Cr-W coating on HCCI. Post-deposition heat treatment resulted in the precipitation of M<sub>7</sub>C<sub>3</sub> carbides, the carbide precipitation led to a substantial increase in the coating hardness to 1240–1445 HV<sub>0.05</sub>. Thus, M<sub>7</sub>C<sub>3</sub> carbides are important for HCCI.

M<sub>7</sub>C<sub>3</sub> (M = Fe, Cr or other element) carbides are the main hardening phases in HCCI, showing a high hardness, a high strength, a high elastic moduli and a ductile property [8].

Furthermore,  $M_7C_3$  carbides enhance the mechanical properties and oxidation resistance of HCCI at high temperatures [9]. The effect mechanism of alloy elements on the structure and mechanical properties of  $M_7C_3$  has been comprehensively studied by first principles calculations [10–14]. Experiments from Coronado [15] showed that  $M_7C_3$  carbides in HCCI were rod-like single crystals with strong anisotropy. The abrasion resistance of the  $M_7C_3$  carbides in the transverse section ([0001] direction) was higher than in the longitudinal section (non-[0001] direction) [15]. Moreover, the wear resistance of ZTA<sub>P</sub>/HCCI composites with a honeycomb structure was higher than High-Chromium Cast Iron [16,17]. Therefore, the extensive application of  $M_7C_3$  multi-component carbides is of great significance to future wear-resistant materials.

One method to improve the hardness and the wear resistance would be to add alloying elements in HCCI, such as vanadium, tungsten, titanium and niobium [18]. As a strong carbide-forming element, tungsten could improve the wear resistance of HCCI [19]. The extensive experiments on the effect of tungsten on microstructure and properties of HCCI have been published over the past few decades [18–21]. Cortés-Carrillo et al. [18] analyzed the effects of tungsten on the microstructure, hardness, microhardness and abrasive wear of High-Chromium Cast Iron with 17 wt % Cr. The results showed that when tungsten content was 4 wt %, the hardness of the alloys increased due to the dispersion of tungsten into the matrix and the  $M_7C_3$  carbides. When the added amount of tungsten exceeded 4 wt %,  $M_2C$  and  $M_6C$  carbides appear in the microstructure of the alloy. The work from Lv et al. [19] found that tungsten considerably improved the wear resistance of HCCI, and the wear resistance of HCCI with 1.03 wt % W increased by 205% compared to HCCI without tungsten. Results from Anijdan et al. [20] also showed that the wear resistance of High-Chromium Cast Iron increased after adding the tungsten. The experimental results from Guerra et al. [21] verified that tungsten partially distributed in the different phases, increasing the microhardness and refining the eutectic carbides. However, the effects of tungsten on the structure and mechanical properties of  $M_7C_3$  are not yet clear and should be further explored to reveal the mechanism.

First principles calculations are an effective way to reveal the mechanism. Zhang et al. [8] investigated the optimization of mechanical properties of  $Fe_{7-x}Cr_xC_3$  carbides by first principles calculations, including  $Fe_6CrC_3$ ,  $Fe_4Cr_3C_3$ ,  $Fe_3Cr_4C_3$  and  $FeCr_6C_3$ , but they ignored  $M_7C_3$  carbides. Chong et al. [22] designed the anisotropic mechanical properties of  $M_7X_3$  ( $M = Fe, Cr, W, Mo$ ,  $X = C, B$ ) by multi-alloying. The results showed that the ductility could be increased by doping of  $W + B$  and  $W + Mo$  without sacrificing the mechanical modulus of  $Cr_4Fe_3C_3$ , and the hardness of  $Cr_4Fe_3C_3$  could be improved by doping of  $Mo + B$  and  $Mo + W + B$  with a finite decrease in ductility. The anisotropy of  $M_7C_3$  carbides is important in the performance of High-Chromium Cast Iron [23]. However, the effect of tungsten on the anisotropy has not been researched and the mechanism is not clear to date. In addition, unfortunately, the stability, properties and electronic structure of  $M_7C_3$  ( $M = Fe, Cr, W$ ) carbides are seldom comprehensively investigated in the literature.

Therefore, the electronic structures, stability, chemical bonds and existing form of  $M_7C_3$  ( $M = Fe, Cr$  and  $W$ ) in Fe—26.8 wt % Cr—3.62 wt % C—2.13 wt % W High-Chromium Cast Iron were thoroughly investigated by first principles calculation experiments, which are helpful to improve the whole performance of HCCI.

## 2. Experimental Details

### 2.1. Calculation Details

First principles calculations are an effective way of investigating the electronic structures, stability and chemical bonds of  $M_7C_3$  carbides in HCCI. The Density Functional Theory (DFT) calculation based on the pseudopotential plane-wave within the Generalized Gradient Approximation (GGA), as implemented in the Cambridge Serial Total Energy Package (CASTEP), was performed in the present work. The Broyden–Fletcher–Goldfarb–Shanno (BFGS) algorithm [24] was applied in the relaxation process of models to optimize the structures. In the structural optimization process, the maximal displacement was

$11.0 \times 10^{-3} \text{ \AA}$ , the largest force was  $0.03 \text{ eV/\AA}$  and the energy change convergence value was less than  $1 \times 10^{-5} \text{ eV/atom}$ . After convergence tests, the cutoff energy of 360 eV and k-point of  $8 \times 8 \times 8$  were selected for these carbides. Although Fang et al. [25] demonstrated that orthorhombic  $\text{Fe}_7\text{C}_3$  is more stable than an orthorhombic or hexagonal structure, Chong et al. [22] found that the crystal structure of  $(\text{Cr, Fe})_7\text{C}_3$  carbides is hexagonal with the space group of  $\text{P6}_3\text{mc}$  (No. 186) by XRD and TEM analysis. Therefore, a hexagonal structure was selected in this work. Zhang et al. [8] investigated the mechanical properties of  $\text{Fe}_{7-x}\text{Cr}_x\text{C}_3$  carbides based on first principles calculations, including  $\text{Fe}_6\text{CrC}_3$ ,  $\text{Fe}_4\text{Cr}_3\text{C}_3$ ,  $\text{Fe}_3\text{Cr}_4\text{C}_3$  and  $\text{FeCr}_6\text{C}_3$ , but they neglected to calculate the other type,  $\text{M}_7\text{C}_3$  carbides. Therefore, the properties of  $\text{Fe}_5\text{Cr}_2\text{C}_3$ ,  $\text{Fe}_2\text{Cr}_5\text{C}_3$  and  $\text{Fe}_3\text{Cr}_4\text{C}_3$  (the crystal structure shown in Figure 1) were calculated by first principles, and the results were compared to the calculated results from references [8,22]. To study the influencing mechanism of tungsten on the structure and mechanical properties of  $\text{M}_7\text{C}_3$ , different amounts of tungsten were doped into  $\text{M}_7\text{C}_3$  carbides. The  $\text{M}_7\text{C}_3$  structures consist of nonequivalent Fe (Cr) atoms, and the lattice parameters, elastic moduli, etc., depend strongly on the substitution sites. We calculated all the formation energy of various sites of doped atoms in the unit cell, and then the unit cell obtained by the minimum formation energy was selected as the final result. Some unit cells of  $\text{M}_7\text{C}_3$  carbides with crystal structures were built, including of  $\text{Fe}_3\text{Cr}_{3.5}\text{W}_{0.5}\text{C}_3$ ,  $\text{Fe}_3\text{Cr}_3\text{W}_1\text{C}_3$ ,  $\text{Fe}_3\text{Cr}_{2.5}\text{W}_{1.5}\text{C}_3$  and  $\text{Fe}_3\text{Cr}_2\text{W}_2\text{C}_3$ , as shown in Figure 1.

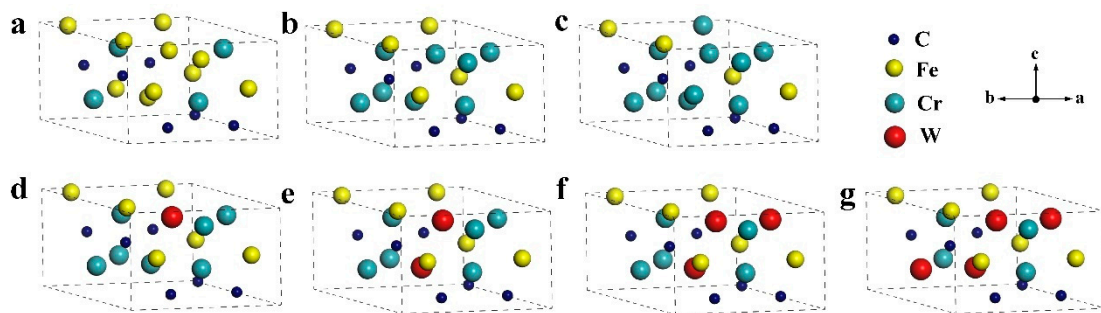


**Figure 1.** Unit cells of  $\text{M}_7\text{C}_3$  carbides with crystal structures: (a)  $\text{Fe}_5\text{Cr}_2\text{C}_3$ ; (b)  $\text{Fe}_3\text{Cr}_4\text{C}_3$ ; (c)  $\text{Fe}_2\text{Cr}_5\text{C}_3$ ; (d)  $\text{Fe}_3\text{Cr}_{3.5}\text{W}_{0.5}\text{C}_3$ ; (e)  $\text{Fe}_3\text{Cr}_3\text{W}_1\text{C}_3$ ; (f)  $\text{Fe}_3\text{Cr}_{2.5}\text{W}_{1.5}\text{C}_3$ ; (g)  $\text{Fe}_3\text{Cr}_2\text{W}_2\text{C}_3$ .

## 2.2. Experimental Data

In this work, Q235 carbon steel with a chemical composition of Fe-0.18% wt % C-0.22% wt % Si-0.45% wt % Mn-0.02% wt % P-0.02% wt % S was used as the substrate, and the cladding materials were High-Chromium Cast Iron powders and tungsten powders (70 wt % W and 29 wt % Fe). The diameter of the above powders was 75–105  $\mu\text{m}$ . The cladding layer was made by an IPG fiber laser system (YLS-6000) with a continuous wave, with a laser beam size of 5 mm  $\times$  5 mm. The parameters were as follows: powder feeding rate  $k = 15 \text{ g/min}$ , scanning speed  $v = 4 \text{ mm/s}$ , laser power  $P = 2000 \text{ W}$ , flow rate of high-purity argon shielding gas = 15 L/min.

The microstructures were observed using a JEM-2100F Transmission Electron Microscope (TEM, manufacturer, city, country) with an energy-dispersive X-ray (EDX, manufacturer, city, country). TEM samples were prepared by ion milling. The wear resistance of the cladding layer was tested by a MM-200 block-on-ring wear testing machine (manufacturer, city, country, the working principle of machine can be found in reference [26]). In situ nanoindentation experiments were performed using the NanoFlip InForce 50 (manufacturer, city, country) to investigate the hardness and modulus of  $\text{M}_7\text{C}_3$  carbides.

For the wear resistance of HCCI, the reported value of weight loss is the average of five results. All data graphs were drawn by Origin 8.0 software, and show the formation energy, mechanical properties, hardness and modulus and weight loss.

### 3. Results and Discussion

#### 3.1. The Equilibrium Lattice Constants and Stability

To ensure the accuracy of the calculation, the optimized lattice constants were calculated, and the calculated results were compared to other calculated results and experimental values, as shown in Table 1. The optimized lattice constants of  $\text{Fe}_3\text{Cr}_4\text{C}_3$  were 6.8358, 6.8358 and 4.5471 Å, which are similar to other calculated values [8] and experimental values [9] (error less than 1.2%). Considering the differences in experimental equipment and calculation methods, it was proved that the parameters adopted were reliable. With the increase in Cr content, the equilibrium lattice parameter  $a$  increased and  $c$  decreased, meaning that  $a$  decreases when  $c$  increases, which is consistent with the conclusion of reference [22]. With the increase in tungsten content, the equilibrium lattice parameters  $a$  and  $b$  gradually increased. The calculated result of equilibrium cell volume (185.61 Å<sup>3</sup>) for  $\text{Fe}_3\text{Cr}_4\text{C}_3$  was similar to the calculated values (181.09 Å<sup>3</sup>) from Zhang et al. [8] (error less than 3%). With the increase in tungsten content, the equilibrium cell volumes and the density gradually increased.

**Table 1.** The lattice parameters of different  $\text{M}_7\text{C}_3$  carbides.

Species	Space Group	a (Å)	b (Å)	c (Å)	Volume (Å <sup>3</sup> )	Density (g/cm <sup>3</sup> )
$\text{Fe}_5\text{Cr}_2\text{C}_3$	P6 <sub>3</sub> mc (186)	7.0054	7.0054	4.3188	183.00	7.61
$\text{Fe}_2\text{Cr}_5\text{C}_3$	P6 <sub>3</sub> mc (186)	6.7795	6.7795	4.6500	187.21	7.23
$\text{Fe}_3\text{Cr}_4\text{C}_3$	P6 <sub>3</sub> mc (186)	6.8358	6.8358	4.5471	185.61	7.37
$\text{Fe}_3\text{Cr}_4\text{C}_3$ [11]	P6 <sub>3</sub> mc (186)	6.8258	6.8258	4.4948	180.0	7.48
$\text{Fe}_3\text{Cr}_4\text{C}_3$ [8]	P6 <sub>3</sub> mc (186)	–	–	–	181.09	–
$\text{Fe}_3\text{Cr}_4\text{C}_3\text{Exp.}$ [11]	P6 <sub>3</sub> mc (186)	6.9	–	4.52	–	–
$\text{Fe}_3\text{Cr}_{3.5}\text{W}_{0.5}\text{C}_3$	P6 <sub>3</sub> mc (186)	6.7556	6.7558	4.8070	190.12	8.34
$\text{Fe}_3\text{Cr}_3\text{W}_1\text{C}_3$	P6 <sub>3</sub> mc (186)	6.8609	6.8609	4.8098	195.45	9.23
$\text{Fe}_3\text{Cr}_{2.5}\text{W}_{1.5}\text{C}_3$	P6 <sub>3</sub> mc (186)	6.8998	6.9721	4.7962	199.98	10.12
$\text{Fe}_3\text{Cr}_2\text{W}_2\text{C}_3$	P6 <sub>3</sub> mc (186)	6.9818	6.9818	4.8382	203.78	11.00

In order to predict whether  $\text{M}_7\text{C}_3$  (M = Fe, Cr and W) carbides were easy to compound, the formation energy was calculated by the following equation [8]:

$$\Delta E_{\text{M}_7\text{C}_3} (\text{M} = \text{Fe, Cr, W}) = E_{\text{tot}}(\text{M}_7\text{C}_3) - xE_{\text{tot}}(\text{Fe}) - yE_{\text{tot}}(\text{Cr}) - zE_{\text{tot}}(\text{W}) - 3E_{\text{tot}}(\text{C}) \quad (1)$$

where  $E_{\text{tot}}(\text{M}_7\text{C}_3)$ ,  $E_{\text{tot}}(\text{Fe})$ ,  $E_{\text{tot}}(\text{Cr})$ ,  $E_{\text{tot}}(\text{W})$  and  $E_{\text{tot}}(\text{C})$  are the total energies of  $\text{M}_7\text{C}_3$  carbides, Fe, Cr, W and C systems, respectively.  $\Delta E_{\text{M}_7\text{C}_3} (\text{M} = \text{Fe, Cr, W})$  is the formation energy of  $\text{M}_7\text{C}_3$  carbides. The formation energy can describe the relative stability of these carbides. If  $\Delta E_{\text{M}_7\text{C}_3} > 0$ , the crystal is unstable or metastable; if  $\Delta E_{\text{M}_7\text{C}_3} < 0$ , the crystal can exist stably [27]. Additionally, if the stability of carbides is better, the carbides may be synthesized easily; if the  $\text{M}_7\text{C}_3$  carbides are not stable, it may not be easy to compound them in the experimental stage [28]. According to Equation (1), the formation energies of  $\text{M}_7\text{C}_3$  carbides were calculated, as shown in Figure 2. Except for  $\text{Fe}_7\text{C}_3$ , the formation energies of other carbides are less than zero, indicating that they are stable crystal structures. With the increase in W and Cr content, the formation energy was increased gradually, indicating that the stability of carbides increased with W and Cr content.

#### 3.2. Mechanical Properties

$\text{M}_7\text{C}_3$  carbides are the main hard phases in wear-resistant material, so the elastic of  $\text{M}_7\text{C}_3$  compounds has an important role in the application of wear-resistant material. The elastic constants  $C_{ij}$  depend mainly on the response of the crystal to external forces, and can be calculated by the bulk, shear and Young's modulus, Poisson's ratio, etc. The bulk modulus and the shear modulus can be calculated by the following method [29]:

$$B_V = \left(\frac{1}{9}\right) [2(C_{11} + C_{12}) + 4C_{13} + C_{33}] \quad (2)$$

$$G_V = \left(\frac{1}{30}\right) [(C_{11} + C_{12} + 2C_{33} - 4C_{13} + 12C_{44} + 12C_{66})] \quad (3)$$

$$B_R = [(C_{11} + C_{12}) C_{33} - 2C_{13}^2] / (C_{11} + C_{12} + 2C_{33} - 4C_{13}) \quad (4)$$

$$G_R = \left(\frac{5}{2}\right) [(C_{11} + C_{12}) C_{33} - 2C_{13}^2] C_{44} C_{66} / \{3B_V C_{44} C_{66} + [(C_{11} + C_{12}) C_{33} - 2C_{13}^2] (C_{44} + C_{66})\} \quad (5)$$

$$B = (B_V + B_R) / 2 \quad (6)$$

$$G = (G_V + G_R) / 2 \quad (7)$$

$$E = 9BG / (3B + G) \quad (8)$$

$$\sigma = (3B - 2G) / (6B + 2G) \quad (9)$$

where  $B$  and  $G$  are the bulk modulus and the shear modulus, respectively.  $E$  and  $\sigma$  are Young's modulus and Poisson's ratio, respectively.  $C_{11}$ ,  $C_{22}$  and  $C_{33}$  represent the uniaxial deformation along the  $[\bar{1}2\bar{1}0]$ ,  $[2\bar{1}\bar{1}0]$  and  $[0001]$  directions, respectively.  $C_{44}$ ,  $C_{55}$  and  $C_{66}$  represent the pure shear deformation on  $(\bar{1}2\bar{1}0)$ ,  $(2\bar{1}\bar{1}0)$  and  $(0001)$  crystal planes, respectively.  $C_{12}$  is the shear deformation on the  $(\bar{1}100)$  crystal plane along the  $[1\bar{1}00]$  direction.

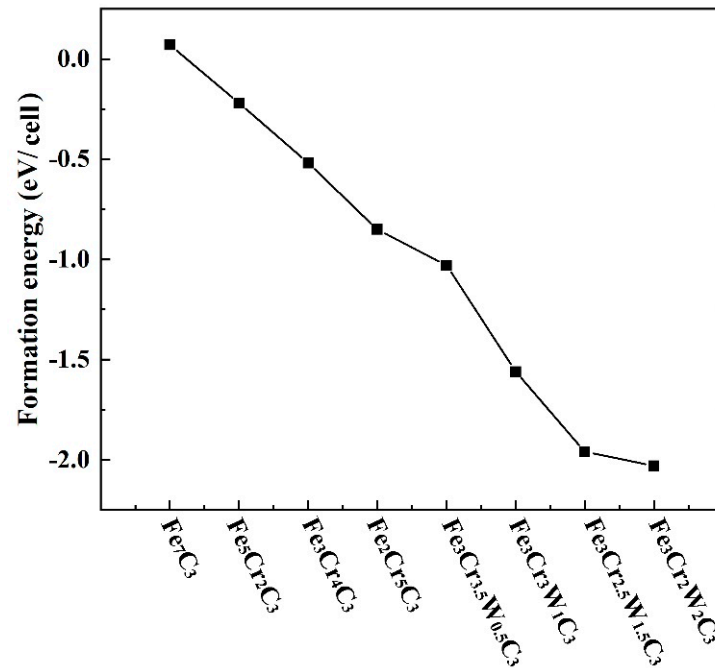


Figure 2. Calculated formation energy of  $M_7C_3$  carbides ( $\Delta E$  for, eV/cell).

For the hexagonal phase, the mechanical stability criteria are given by [29]:

$$C_{44} > 0, C_{11} > |C_{12}|, (C_{11} + 2C_{12})C_{33} > 2C_{13} \quad (10)$$

The calculated elastic constants of  $M_7C_3$  carbides satisfied the above formula, indicating that these  $M_7C_3$  carbides were stable structures. Table 2 lists the calculated elastic constants ( $C_{ij}$ ) of different  $M_7C_3$  carbides, which showed good agreement with the data of other researchers [22]. The largest  $C_{11}$ ,  $C_{12}$  and  $C_{13}$  appeared on  $Fe_3Cr_2W_2C_3$ , but the largest  $C_{66}$  and  $C_{44}$  appeared on  $Fe_2Cr_5C_3$ . Because the hardness of  $M_7C_3$  carbides is large, the relatively simple semi-empirical equation of hardness can be used, which is [30]:

$$H_V = 1.92 K^{1.137} G^{0.708}, K = G/B \quad (11)$$

Figure 3 shows the mechanical properties of  $M_7C_3$  carbides. The shear modulus and Young's modulus of  $Fe_2Cr_5C_3$  are the largest. With the addition of tungsten, the shear modulus and Young's modulus began to decrease, indicating that the alloying tungsten decreases the strength of  $M_7C_3$ . Poisson's ratio can reflect the flexibility; the larger Poisson's ratio is, the softer the material is. Poisson's ratio of  $Fe_3Cr_{2.5}W_{1.5}C_3$  is the largest, indicating that the  $Fe_3Cr_{2.5}W_{1.5}C_3$  compound is the softest. Pugh's modulus ratio  $B/G$  and Cauchy pressure ( $C_{11}-C_{44}$ ) can explain the ductile/brittle properties. When  $G/B$  is smaller than 0.571, the  $M_7C_3$  has good ductile property [8]. With the addition of tungsten,  $G/B$  is reduced, indicating that tungsten can improve the toughness of  $M_7C_3$ . Cauchy pressure of  $M_7C_3$  carbides increased with tungsten content, as shown in Figure 3f, which indicates that tungsten doping can improve the ductility of  $(Fe, Cr)_7C_3$  carbides. The composition of  $(Fe, Cr, W)_7C_3$  is expected to be a high hardness and softness material; thus, the synthesis of this carbide would be of great interest.

**Table 2.** The elastic constants ( $C_{ij}$ , GPa) of different  $M_7C_3$  carbides.

Species	$C_{11}$	$C_{33}$	$C_{44}$	$C_{12}$	$C_{13}$	$C_{66}$
$Fe_5Cr_2C_3$	534.6	560.8	123.8	193.5	255.4	152.3
$Fe_2Cr_5C_3$	562.1	559.2	157.9	159.2	258.3	193.0
$Fe_3Cr_4C_3$	549.2	531.6	122.5	179.6	248.1	179.6
$Fe_3Cr_4C_3$ [9]	550.7	532.8	110.6	185.2	229.0	182.7
$Fe_3Cr_{3.5}W_{0.5}C_3$	546.1	523.6	100.9	251.5	246.0	166.5
$Fe_3Cr_3WC_3$	543.2	504.9	99.1	236.8	243.6	155.8
$Fe_3Cr_3WC_3$ [9]	565.5	415.4	87.8	252.0	249.2	156.8
$Fe_3Cr_{2.5}W_{1.5}C_3$	578.9	403.4	92.3	276.5	279.5	149.1
$Fe_3Cr_2W_2C_3$	581.5	377.5	90.9	300.1	288.1	166.9

Anisotropy of  $M_7C_3$  effects the wear resistance of HCCI [8]. Therefore, the analysis of anisotropy is important for understanding the properties of  $M_7C_3$  carbides. The anisotropy of Young's modulus for hexagonal  $M_7C_3$  carbides along different directions is expounded by the 3D surface contours, following [22]:

$$1/E = (1 - l_1^2)^2 S_{11} + l_1^4 S_{33} + l_1^2 (1 - l_1^2) (2S_{13} + S_{44}) \quad (12)$$

where  $S_{ij}$  is the elastic compliance constant.  $S_{ij}$  is the inverse matrix of  $C_{ij}$ .  $l_3 = \cos\varphi$  is the directional cosine. The results are shown in Figure 4. In Figure 4a,b,d,e, it can be seen that  $Fe_5Cr_2C_3$ ,  $Fe_3Cr_4C_3$ ,  $Fe_3Cr_{3.5}W_{0.5}C_3$  and  $Fe_3Cr_3W_1C_3$  showed strong anisotropy. As the Cr content increased, the elastic anisotropy of  $(Fe, Cr)_7C_3$  became weaker. Similarly, as the tungsten content increased, the elastic anisotropy of  $(Fe, Cr, W)_7C_3$  became weaker, as shown in Figure 4f,g. The results indicate that alloying could weaken the elastic anisotropy of  $M_7C_3$  carbides, which is in agreement with other calculated results [22].

### 3.3. The Electronic Structures

As is known, the properties of carbides are associated with electronic states [31]. In order to gain some insight into the nature of bonding in  $M_7C_3$  carbides, the band structure and the Partial Density of States (PDOS) were calculated. Figure 5 shows the band structure of  $M_7C_3$ , and the dashed line indicates the Fermi level. All calculated  $M_7C_3$  carbides in this work exhibited metallic properties. Figure 6 shows the Total Density of States (TDOS) and the Partial Density of States (PDOS). PDOS can analyze the electronic hybridization states quantitatively with chemical bonding.  $Fe_5Cr_2C_3$ ,  $Fe_3Cr_4C_3$ ,  $Fe_2Cr_5C_3$  and  $Fe_3Cr_3W_1C_3$  carbides show large shifts, because the up and down spin channels are not symmetric. However,  $Fe_3Cr_{3.5}W_{0.5}C_3$ ,  $Fe_3Cr_{2.5}W_{1.5}C_3$  and  $Fe_3Cr_2W_2C_3$  are symmetric, which may indicate non-magnetic characteristics of these carbides. In Figure 6, the DOS on both sides of the Fermi level were determined mainly by the Fe-d and Cr-d. From  $-15$  to  $-10$  eV, TDOS mainly consists of C-s orbit, but from  $-7.5$  to  $10$  eV, TDOS of  $M_7C_3$  mainly consists of W-d, Fe-d, Cr-d and C-p orbit, as shown in Figure 6d–g. From  $-7.5$  to  $-2.5$  eV, TDOS

mainly consists of Fe-d, W-d and Cr-d orbit, and their peak shape and peak intensity are similar, indicating that there is orbital hybridization. The d orbit of Cr, Fe, W and the p orbit of carbon have strong hybridization, suggesting a covalent bond between the Cr, Fe, W atom and carbon atom. The total electron density distribution is shown in Figure 7. For an ideal single crystal, the magnitude of the mechanical modulus is related to the chemical bond strength. In Figure 7a, Fe-C-Cr and Fe-C-Fe covalent chains can be observed in  $\text{Fe}_3\text{Cr}_4\text{C}_3$  carbides, which is in agreement with other calculated results [8]. In Figure 7b, Cr-W-C, Fe-C-Cr and Fe-C-W covalent chains can be observed in  $\text{Fe}_3\text{Cr}_2\text{W}_2\text{C}_3$  carbides, explaining the decrease in formation energy after adding tungsten.

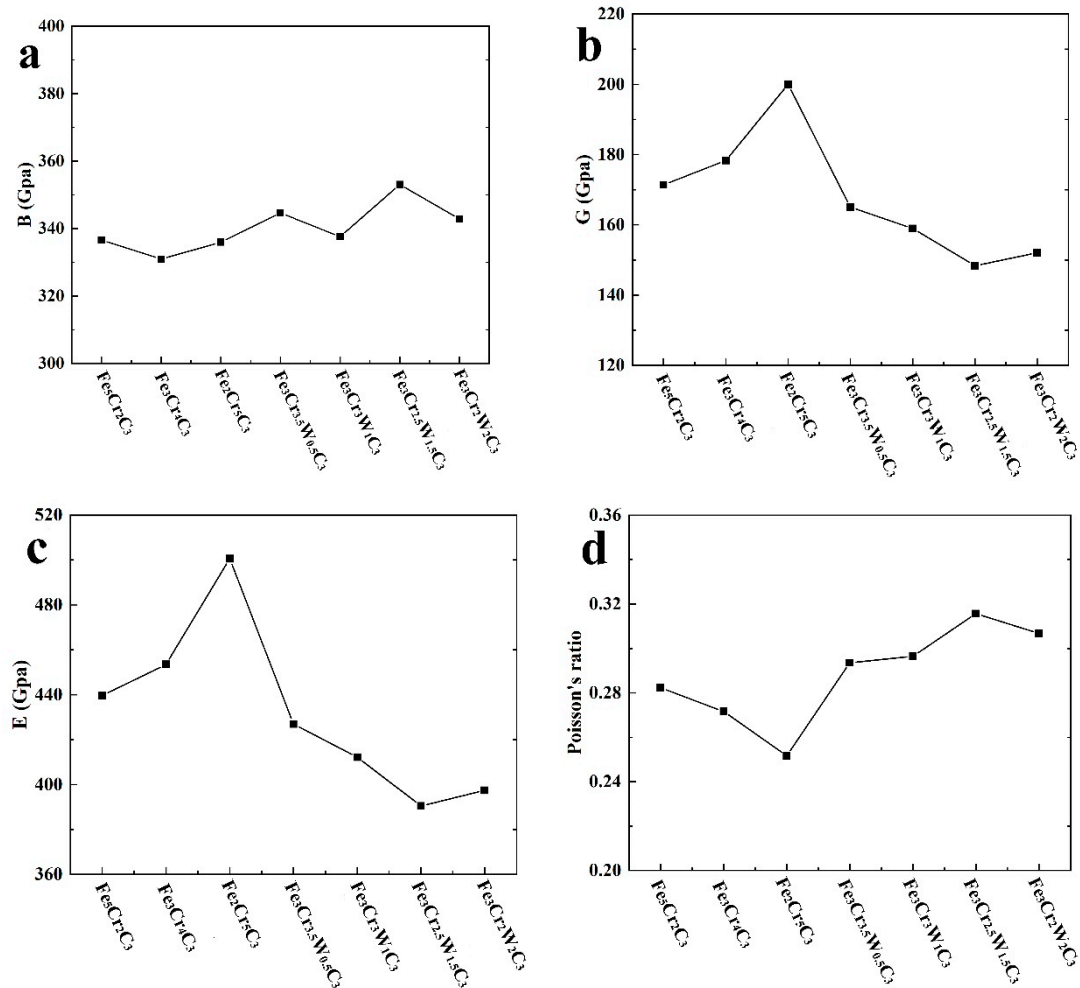
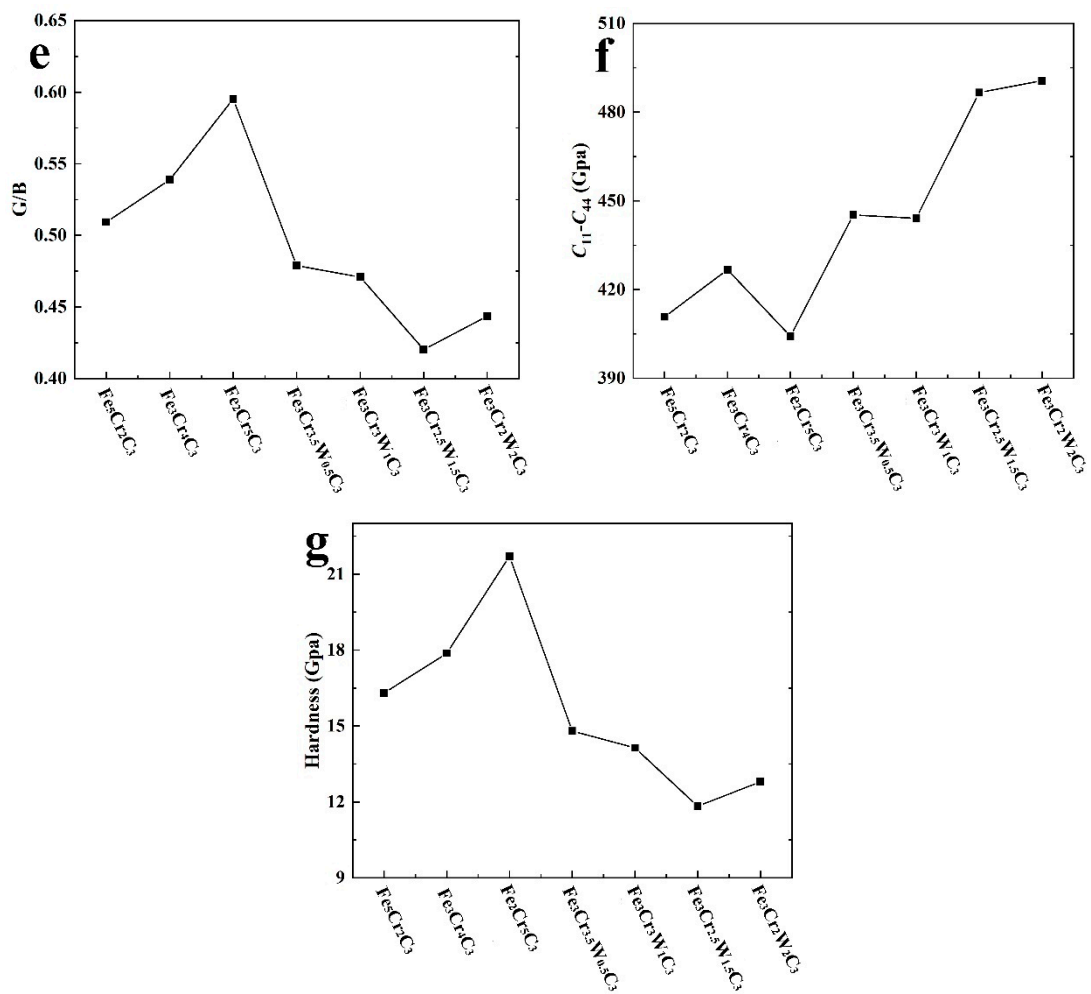
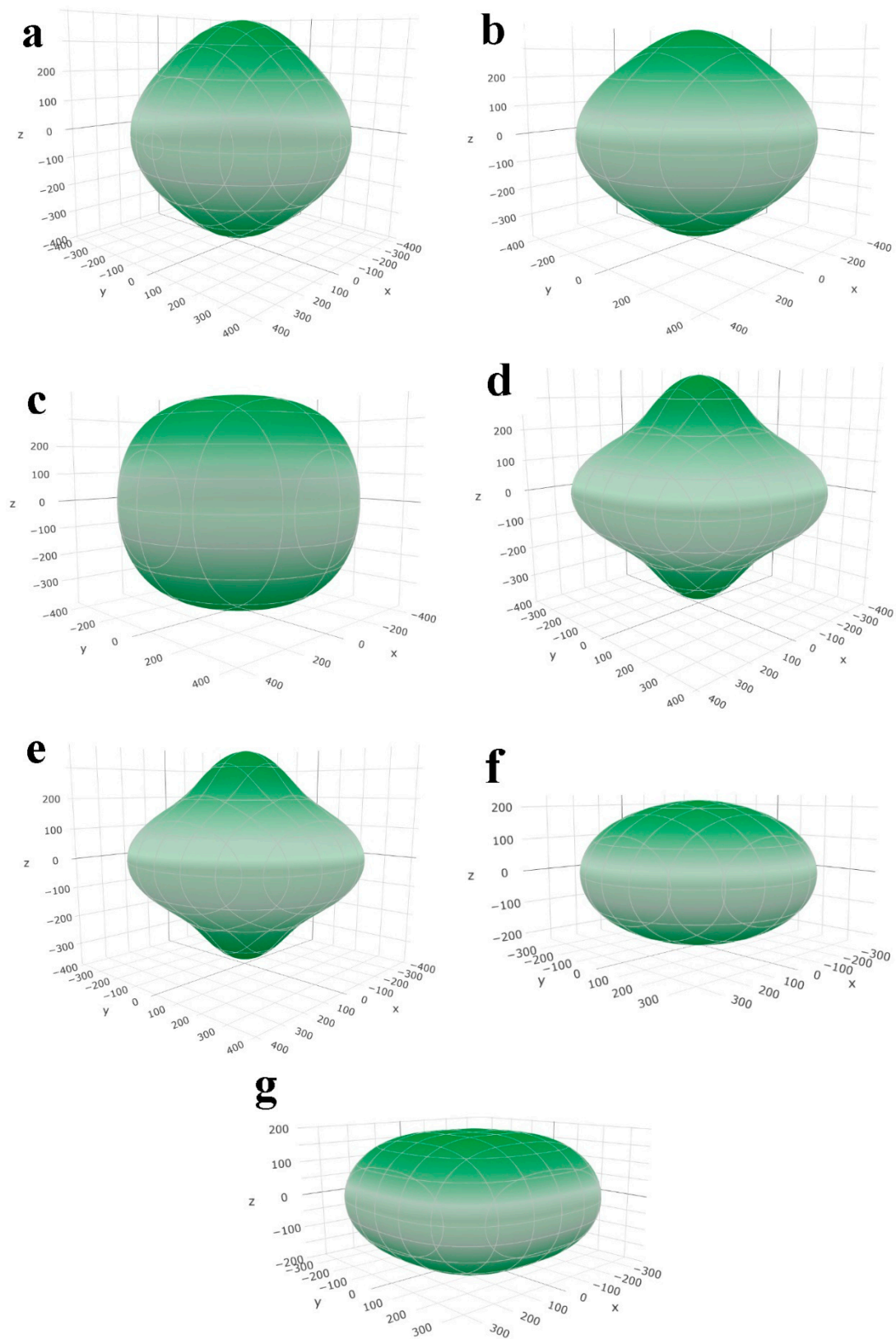


Figure 3. Cont.



**Figure 3.** The mechanical properties of  $M_7C_3$ : (a) the bulk modulus (B); (b) the shear modulus (G); (c) Young's modulus (E); (d) Poisson's ratio ( $\sigma$ ); (e) Pugh's modulus ratio G/B; (f) Cauchy pressure  $C_{12}-C_{44}$ ; (g) calculated hardness.



**Figure 4.** Surface constructions of Young's modulus of  $M_7C_3$  carbides: (a)  $Fe_5Cr_2C_3$ ; (b)  $Fe_3Cr_4C_3$ ; (c)  $Fe_2Cr_5C_3$ ; (d)  $Fe_3Cr_{3.5}W_{0.5}C_3$ ; (e)  $Fe_3Cr_3W_1C_3$ ; (f)  $Fe_3Cr_{2.5}W_{1.5}C_3$ ; (g)  $Fe_3Cr_2W_2C_3$ .

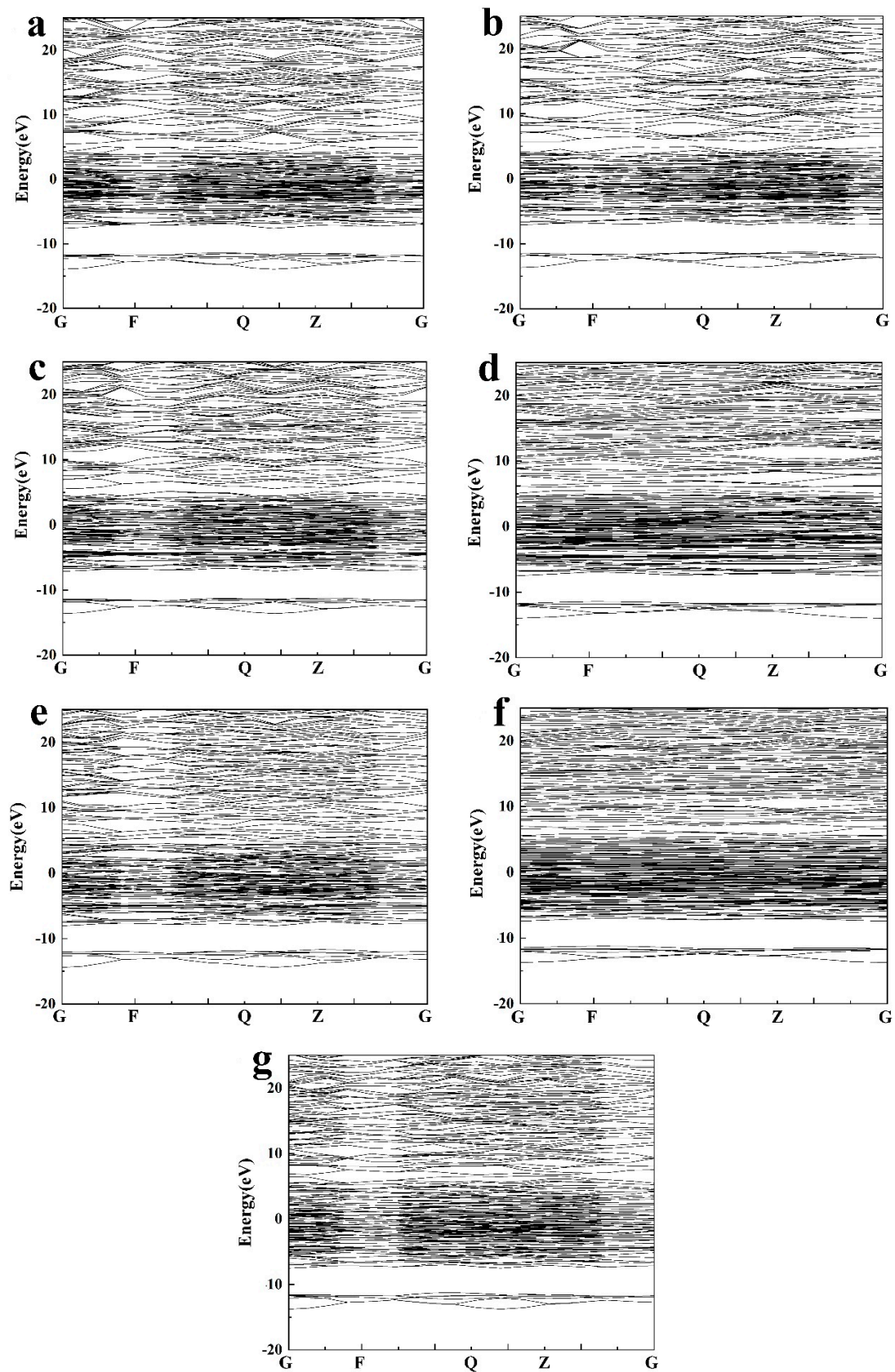


**Figure 5.** Calculated band structure: (a)  $\text{Fe}_5\text{Cr}_2\text{C}_3$ ; (b)  $\text{Fe}_3\text{Cr}_4\text{C}_3$ ; (c)  $\text{Fe}_2\text{Cr}_5\text{C}_3$ ; (d)  $\text{Fe}_3\text{Cr}_{3.5}\text{W}_{0.5}\text{C}_3$ ; (e)  $\text{Fe}_3\text{Cr}_3\text{W}_1\text{C}_3$ ; (f)  $\text{Fe}_3\text{Cr}_{2.5}\text{W}_{1.5}\text{C}_3$ ; (g)  $\text{Fe}_3\text{Cr}_2\text{W}_2\text{C}_3$ .

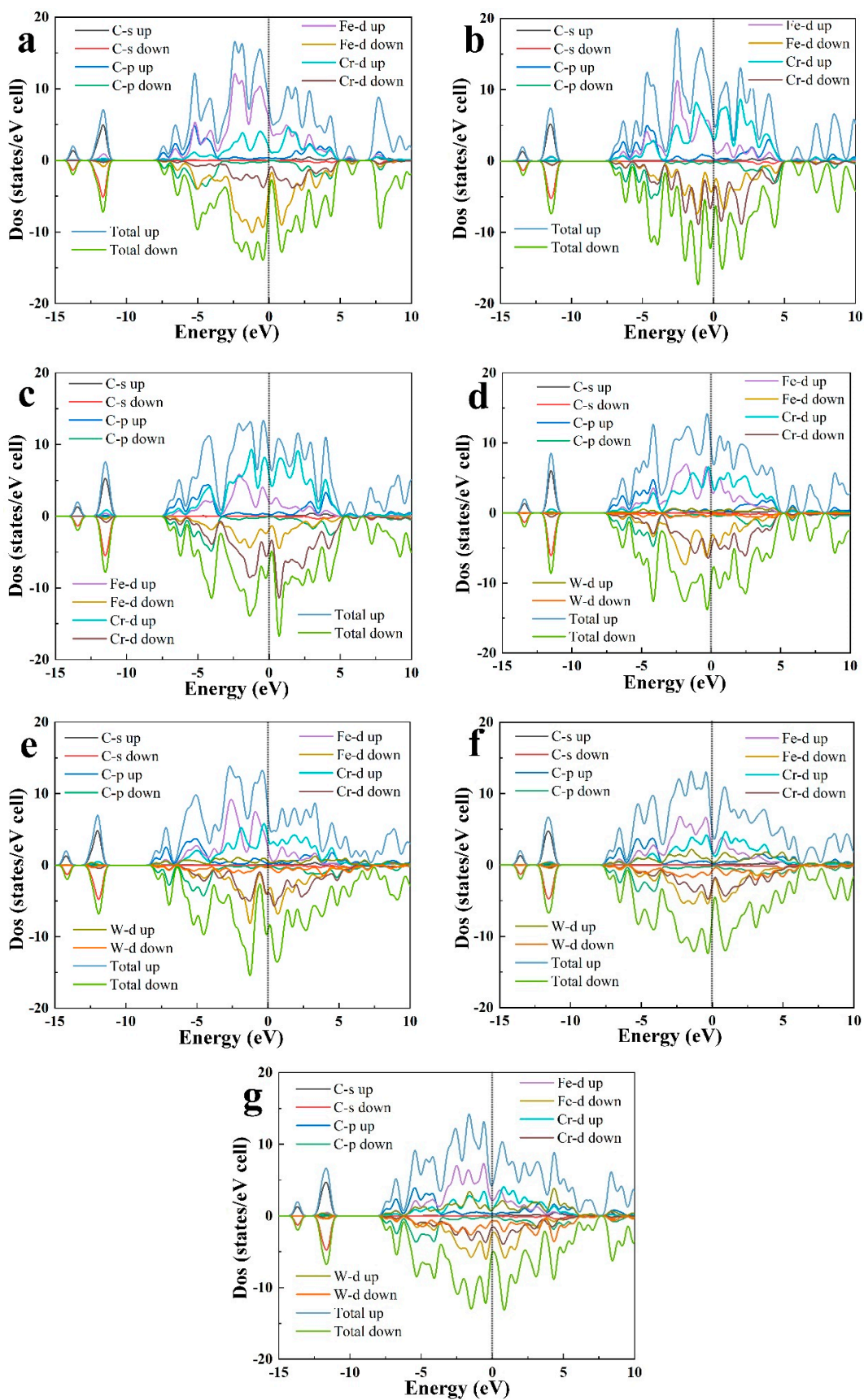
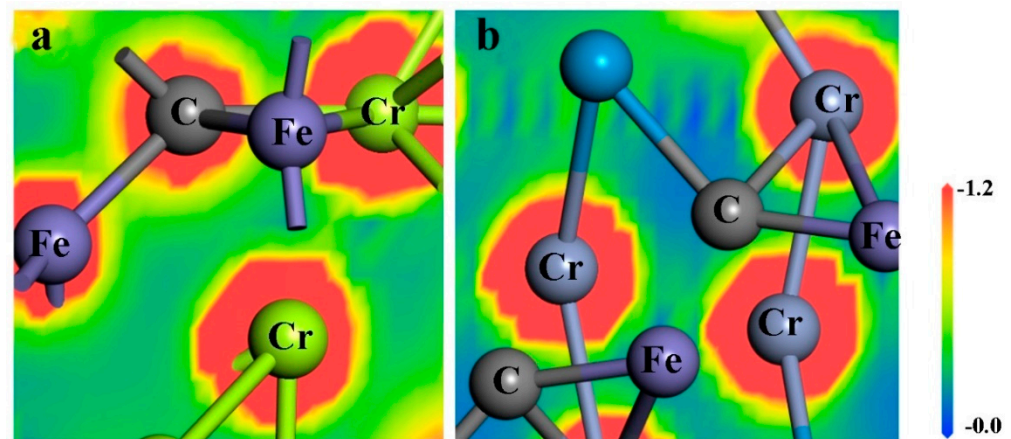


Figure 6. Calculated PDOS: (a)  $\text{Fe}_5\text{Cr}_2\text{C}_3$ ; (b)  $\text{Fe}_3\text{Cr}_4\text{C}_3$ ; (c)  $\text{Fe}_2\text{Cr}_5\text{C}_3$ ; (d)  $\text{Fe}_3\text{Cr}_{3.5}\text{W}_{0.5}\text{C}_3$ ; (e)  $\text{Fe}_3\text{Cr}_3\text{W}_1\text{C}_3$ ; (f)  $\text{Fe}_3\text{Cr}_{2.5}\text{W}_{1.5}\text{C}_3$ ; (g)  $\text{Fe}_3\text{Cr}_2\text{W}_2\text{C}_3$ .



**Figure 7.** The valence electron density for (a)  $\text{Fe}_3\text{Cr}_4\text{C}_3$  and (b)  $\text{Fe}_3\text{Cr}_2\text{W}_2\text{C}_3$ .

### 3.4. TEM Analysis

To study the existence form of carbides after adding tungsten to HCCL, the microstructures of High-Chromium Cast Iron with a composition of 3.44C-26.7Cr-1.25Mn-2.3 wt % W was characterized by TEM. Figure 8a shows the bright-field TEM micrographs, and Figure 8b shows the Selected Area Diffraction Pattern (SADP) of  $\text{M}_7\text{C}_3$ . The results show that the carbides are  $\text{M}_7\text{C}_3$  phase with a hexagonal structure, and the space group is  $\text{P6}_3\text{mc}$  (No. 186). According to the accurate measurement using EDX at 10 different areas of  $\text{M}_7\text{C}_3$ , the calculated analysis suggests that  $(\text{Fe}, \text{Cr}, \text{W})_7\text{C}_3$  has a stoichiometry of  $(\text{Fe}_{3.27}\text{Cr}_{2.99}\text{W}_{0.74})\text{C}_3$ . Moreover, the lattice constant of  $(\text{Fe}_{3.27}\text{Cr}_{2.99}\text{W}_{0.74})\text{C}_3$  carbides is  $a = 0.6833$  nm,  $b = 0.6833$  nm,  $c = 0.4796$  nm.

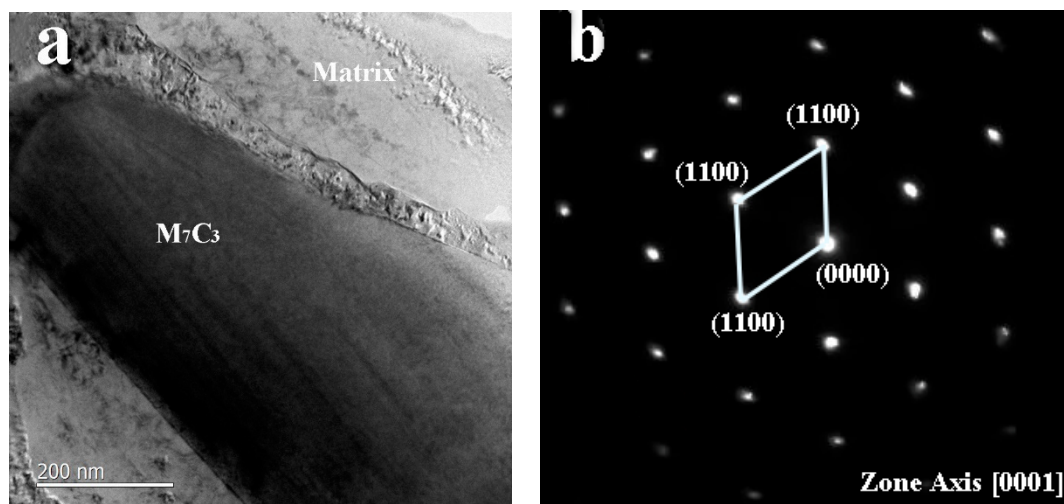


**Figure 8.** Bright-field TEM micrographs and corresponding Selected Area Diffraction Patterns (SADPs): (a) bright-field TEM micrographs; (b) corresponding SADPs of  $\text{M}_7\text{C}_3$ .

### 3.5. Nanoindentation Experiments

The hardness and modulus of carbides were investigated by a NanoFlip InForce 50. Figure 9a,b shows the indentation hardness HIT and the indentation modulus EIT of  $\text{M}_7\text{C}_3$  carbides, respectively. With indentation depths larger than 100 nm, EIT and HIT of  $\text{M}_7\text{C}_3$  phase reached a constant level, which indicated that the intrinsic material properties of the hard phases were measured in this experiment. Furthermore, the crack formation was not observed at an indentation depth of 200 nm, and the triangular indentations could be observed on  $\text{M}_7\text{C}_3$  carbides, indicating that the credibility of the data is high. The indentation hardness values of  $(\text{Fe}, \text{Cr})_7\text{C}_3$  and  $(\text{Fe}, \text{Cr}, \text{W})_7\text{C}_3$  were 17.55 and 17.39 GPa,

respectively. The indentation modulus values of  $(\text{Fe, Cr})_7\text{C}_3$  and  $(\text{Fe, Cr, W})_7\text{C}_3$  were 367.87 and 385.48 GPa, respectively.

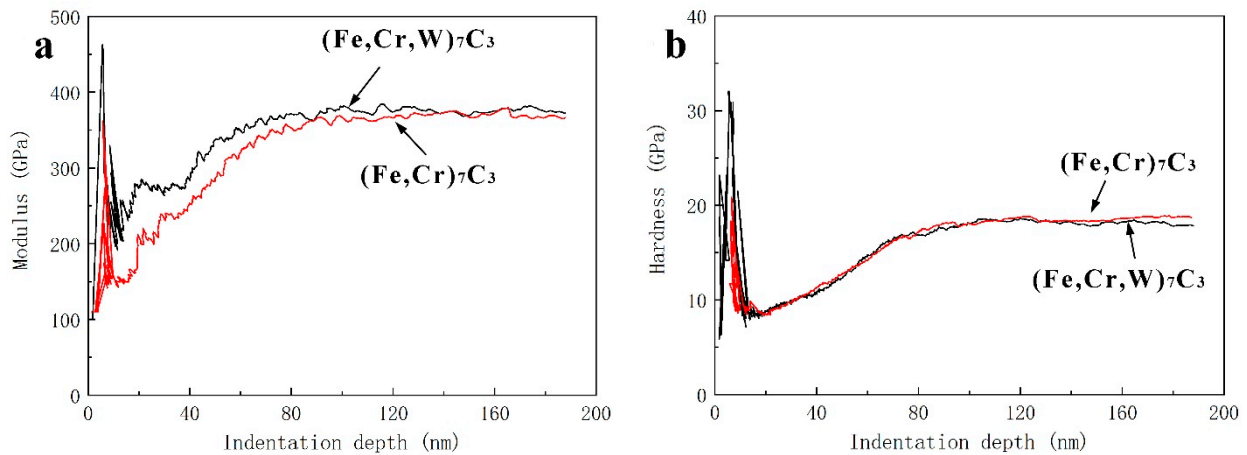


**Figure 9.** Indentation hardness and indentation modulus of  $M_7C_3$  phase: (a) indentation hardness; (b) indentation modulus.

### 3.6. Wear Resistance

The wear resistance of HCCI was tested by a MM-200 block-on-ring wear testing machine. It was apparent that the wear resistance of HCCI after adding tungsten exceeds that of HCCI without tungsten. With the increase in wear load, the wear loss increased, as shown in Figure 10. The wear resistance of HCCI was closely related to the hardness of carbides, but also to the hardness of the matrix. Therefore, the abrasion resistance slightly increased after tungsten was added.

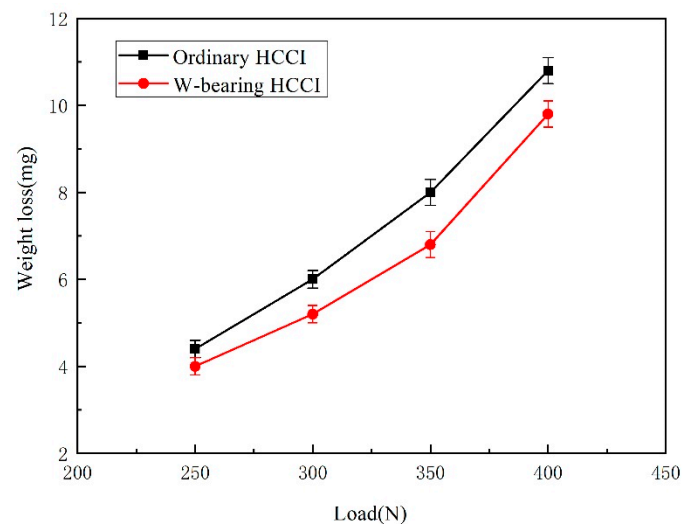


**Figure 10.** The wear resistance of HCCI.

To better reflect the wear resistance of HCCI after the addition of tungsten, the worn surface was characterized by a JSM-6510 Scanning Electron Microscope (SEM) and a VK-9710 color 3D laser scanning microscope. Figure 11a,b is the SEM images of ordinary HCCI and HCCI with tungsten, respectively. Figure 11c,d is the 3D laser morphologies of the worn surfaces of ordinary HCCI and HCCI with tungsten, respectively. Some obvious scratches were found on the specimen surface, and the wear surfaces of both HCCIs were consistent [32]. However, the groove scratches and fine wear of ordinary HCCI were obviously deep, indicating that the wear resistance of HCCI is better after adding tungsten.

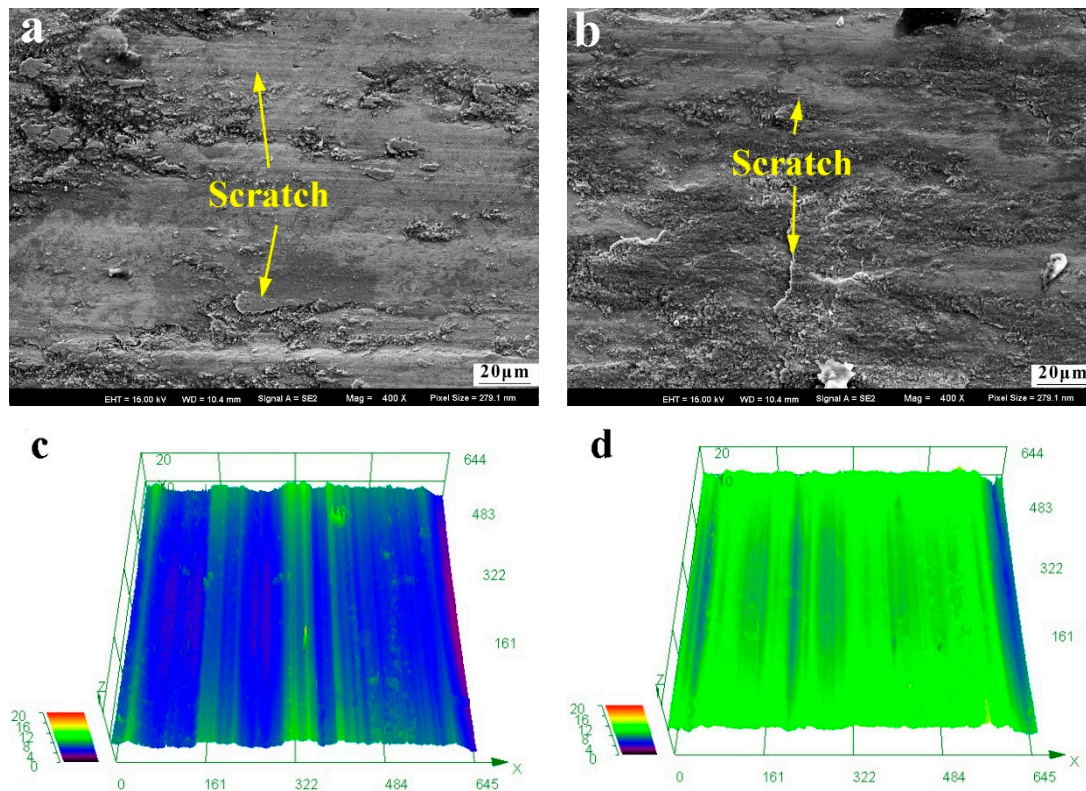


**Figure 11.** The worn surfaces of HCCI: (a,c) ordinary HCCI; (b,d) tungsten-bearing HCCI.

#### 4. Conclusions

In this work, we added tungsten to High-Chromium Cast Iron to investigate the microstructures and properties of  $M_7C_3$  carbides by first principles and experiments.

(a) With the increase in W and Cr content in  $M_7C_3$  carbides, the formation energy of  $M_7C_3$  carbides gradually decreased. Tungsten doping can improve the ductility of  $(Fe, Cr)_7C_3$  carbides, and the composition of  $(Fe, Cr, W)_7C_3$  is expected to be a high hardness and softness material.

(b) TEM results showed that the  $(Fe, Cr, W)_7C_3$  carbides are  $(Fe_{3.27}Cr_{2.99}W_{0.74})C_3$  with a hexagonal structure after adding 2.13 wt % W into Fe—26.8 wt % Cr—3.62 wt % C High-Chromium Cast Iron.

(c) Wear test results showed that the wear resistance could be improved after adding tungsten to HCCI.

**Author Contributions:** C.C.: Investigating, Methodology, Formal analysis, Writing, Review, Editing. J.W.: Supervision, Funding acquisition, Writing, Review, Editing. Y.G.: Investigation, Experiments, Data curation. L.M.: Software, Writing, Review, Editing. All authors have read and agreed to the published version of the manuscript.

**Funding:** This research was supported by the National Natural Science Foundation of China (grant 51875252), the Natural Science Foundation of Heilongjiang Province (LH2020E026) and the Basic Scientific Research Business Fee Project of Heilongjiang Provincial Department of Education (2020-KYYWF-0266).

**Institutional Review Board Statement:** Not applicable.

**Informed Consent Statement:** Not applicable.

**Data Availability Statement:** The datasets generated during and/or analyzed during the current study are available from the corresponding author on reasonable request.

**Conflicts of Interest:** The authors declare no conflict of interest.

## References

1. Giourtas, L.; Brownlie, F.; Hodgkiess, T.; Galloway, A.M. Influence of metallic matrix on erosion-corrosion behaviour of high chromium cast irons under slurry impingement conditions. *Wear* **2021**, *477*, 203834. [[CrossRef](#)]
2. Li, Y.; Shen, D.; Xu, N.; Tong, W. Cladding high chromium cast irons on low carbon steel: Microstructure and mechanical properties. *J. Mater. Res. Technol.* **2020**, *9*, 3856. [[CrossRef](#)]
3. Wiengmoon, A.; Pearce, J.T.H.; Nusen, S.; Chairuangstri, T. Electron microscopy study of carbides precipitated during destabilization and tempering heat treatments of 25 wt.%Cr-0.7 wt.%Mo high chromium cast irons. *Micron* **2021**, *143*, 103025. [[CrossRef](#)] [[PubMed](#)]
4. Nayak, U.P.; Guitar, M.A.; Mücklich, F.A. A Comparative Study on the Influence of Chromium on the Phase Fraction and Elemental Distribution in As-Cast High Chromium Cast Irons: Simulation vs. Experimentation. *Metals* **2020**, *10*, 30. [[CrossRef](#)]
5. Bedolla-Jacuinde, A.; Guerra, F.V.; Guerrero-Pastran, A.J.; Sierra-Cetina, M.A.; Valdez-Medina, S. Microstructural effect and wear performance of high chromium white cast iron modified with high boron contents. *Wear* **2021**, *476*, 203675. [[CrossRef](#)]
6. Heydari, D.; Skandani, A.A.; Haik, M.A. Effect of carbon content on carbide morphology and mechanical properties of A.R. white cast iron with 10-12% tungsten. *Mater. Sci. Eng. A* **2012**, *542*, 113–126. [[CrossRef](#)]
7. Efremenko, V.G.; Chabak, Y.G.; Lekatou, A.; Karantzalis, A.E.; Efremenko, A.V. Pulsed plasma deposition of Fe-C-Cr-W coating on high-Cr-cast iron: Effect of layered morphology and heat treatment on the microstructure and hardness. *Surf. Coat. Technol.* **2016**, *304*, 293–305. [[CrossRef](#)]
8. Zhang, P.; Zhou, Y.; Yang, J.; Li, D.; Ren, X.; Yang, Y.; Yang, Q. Optimization on mechanical properties of Fe<sub>7-x</sub>Cr<sub>x</sub>C<sub>3</sub> carbides by first-principles investigation. *J. Alloys Compd.* **2013**, *560*, 49–53. [[CrossRef](#)]
9. Zhao, Z.; Song, R.; Zhang, Y.; Yu, P.; Pei, Y. Co-orientation relationship between secondary carbides and adjacent ferrite after quenching and tempering in high chromium cast iron. *Vacuum* **2021**, *184*, 109911. [[CrossRef](#)]
10. Xiao, B.; Xing, J.D.; Feng, J.; Zhou, C.T.; Cheng, Y.H. A comparative study of Cr<sub>7</sub>C<sub>3</sub>, Fe<sub>3</sub>C and Fe<sub>2</sub>B in cast iron both from ab initio calculations and experiments. *J. Phys. D* **2009**, *42*, 115415. [[CrossRef](#)]
11. Xiao, B.; Feng, J.; Zhou, C.T.; Xing, J.D.; Xie, X.J.; Chen, Y.H. First principles study on the electronic structures and stability of Cr<sub>7</sub>C<sub>3</sub> type multi-component carbides. *Chem. Phys. Lett.* **2008**, *459*, 129–132. [[CrossRef](#)]
12. Konyaeva, M.A.; Medvedeva, N.I. Electronic structure, magnetic properties, and stability of the binary and ternary carbides (Fe, Cr)<sub>3</sub>C and (Fe, Cr)<sub>7</sub>C<sub>3</sub>. *Phys. Solid State* **2009**, *51*, 2084. [[CrossRef](#)]
13. Music, D.; Kreissig, U.; Mertens, R.; Schneider, J.M. Electronic structure and mechanical properties of Cr<sub>7</sub>C<sub>3</sub>. *Phys. Lett. A* **2004**, *326*, 473. [[CrossRef](#)]
14. Sun, L.; Ji, X.; Zhao, L.; Zhai, W.; Xu, L.; Dong, H.; Liu, Y.; Peng, J. First principles investigation of binary chromium carbides Cr<sub>7</sub>C<sub>3</sub>, Cr<sub>3</sub>C<sub>2</sub> And Cr<sub>23</sub>C<sub>6</sub>: Electronic structures, mechanical properties and thermodynamic properties under pressure. *Materials* **2022**, *15*, 558. [[CrossRef](#)] [[PubMed](#)]
15. Coronado, J.J. Effect of (Fe, Cr)<sub>7</sub>C<sub>3</sub> carbide orientation on abrasion wear resistance and fracture toughness. *Wear* **2011**, *270*, 287–293. [[CrossRef](#)]
16. Zhou, M.; Sui, Y.; Chong, X.; Jiang, Y.H. Wear resistance mechanism of ZTA<sub>p</sub>/HCCI composites with a honeycomb structure. *Metals* **2018**, *8*, 588. [[CrossRef](#)]
17. El-Aziz, K.A.; Zohdy, K.; Saber, D.; Sallam, H.E.M. Wear and corrosion behavior of high-Cr white cast iron alloys in different corrosive media. *J. Bio-Tribo. Corros.* **2015**, *1*, 25. [[CrossRef](#)]
18. Cortés-Carrillo, E.; Bedolla-Jacuinde, A.; Mejía, I.; Zepeda, C.M.; Guerra-Lopez, F.V. Effects of tungsten on the microstructure and on the abrasive wear behavior of a high chromium white iron. *Wear* **2017**, *376-377*, 77–85. [[CrossRef](#)]
19. Lv, Y.; Sun, Y.; Zhao, J.; Yu, G.; Shen, J.; Hu, S. Effect of tungsten on microstructure and properties of high chromium cast iron. *Mater. Des.* **2012**, *39*, 303–308. [[CrossRef](#)]
20. Anijdan, H.S.M.; Bahrami, A.; Varahram, N.; Davami, P. Effects of tungsten on erosion-corrosion behavior of high chromium white cast iron. *Mater. Sci. Eng. A* **2007**, *454*, 623–628. [[CrossRef](#)]
21. Guerra, F.V.; Bedolla-Jacuinde, A.; Zuno-Silva, J.; Mejía, I.; Cardoso-Legorreta, E.; Arenas-Flores, A. Effect of the simultaneous Ti and W addition on the microstructure and wear behavior of a high chromium white cast iron. *Met. Res. Technol.* **2019**, *116*, 602. [[CrossRef](#)]
22. Chong, X.Y.; Hu, M.Y.; Wu, P.; Shan, Q.; Jiang, Y.H.; Li, Z.L.; Feng, J. Tailoring the anisotropic mechanical properties of hexagonal M<sub>7</sub>X<sub>3</sub> (M=Fe, Cr, W, Mo; X=C, B) by multialloying. *Acta Mater.* **2019**, *169*, 193–208. [[CrossRef](#)]
23. Xiao, B.; Feng, J.; Zhou, C.T.; Jiang, Y.H.; Zhou, R. Mechanical properties and chemical bonding characteristics of Cr<sub>7</sub>C<sub>3</sub> type multicomponent carbides. *J. Appl. Phys.* **2011**, *109*, 1–9. [[CrossRef](#)]
24. Fischer, T.H.; Almlof, J. General methods for geometry and wave function optimization. *J. Phys. Chem.* **1992**, *96*, 9768. [[CrossRef](#)]
25. Fang, C.M.; van Huis, M.A.; Zandbergen, H.W. Structural, electronic, and magnetic properties of iron carbide Fe<sub>7</sub>C<sub>3</sub> phases from first-principles theory. *Phys. Rev. B* **2009**, *80*, 224108. [[CrossRef](#)]
26. Yang, P.; Fu, H.; Zhao, X.; Lin, J.; Lei, Y. Wear behavior of CAD1 obtained at different austenitizing temperatures. *Tribol. Int.* **2019**, *140*, 105876.
27. Lin, C.M.; Chang, C.M.; Chen, J.H.; Wu, W. The effects of additive elements on the microstructure characteristics and mechanical properties of Cr-Fe-C hard-facing alloys. *J. Alloys Compd.* **2010**, *498*, 30–36. [[CrossRef](#)]

28. Sun, S.; Fu, H.; Lin, J.; Guo, G.; Lei, Y.; Wang, R. The stability, mechanical properties, electronic structures and thermodynamic properties of (Ti, Nb)C compounds by first principles calculations. *J. Mater. Res.* **2018**, *4*, 495–506. [[CrossRef](#)]
29. Wu, Z.; Zhao, E.; Xiang, H.; Hao, X.; Liu, X.; Meng, J. Crystal structures and elastic properties of superhard IrN<sub>2</sub> and IrN<sub>3</sub> from first principles. *Phys. Rev. B.* **2007**, *76*, 1–15.
30. Tian, Y.; Xu, B.; Zhao, Z. Microscopic theory of hardness and design of novel superhard crystals. *Int. J. Refract. Met. Hard. Mater.* **2012**, *33*, 93–106. [[CrossRef](#)]
31. Ganguly, A.; Murthy, V.; Kannoorpatti, K. Structural and electronic properties of chromium carbides and Fe-substituted chromium carbides. *Mater. Res. Express* **2020**, *7*, 056508. [[CrossRef](#)]
32. Țălu, Ș. Micro and nanoscale characterization of three dimensional surfaces. In *Basics and Applications*; Napoca Star Publishing House: Cluj-Napoca, Romania, 2015; pp. 21–27.